OPEN ACCESS

University of BRISTOL

Barton, DAW., Krauskopf, B., & Wilson, RE. (2005). *Periodic solutions and their bifurcations in a non-smooth second-order delay differential equation*. http://hdl.handle.net/1983/472

Early version, also known as pre-print

Link to publication record in Explore Bristol Research
PDF-document

University of Bristol - Explore Bristol Research
General rights

This document is made available in accordance with publisher policies. Please cite only the published version using the reference above. Full terms of use are available:
http://www.bristol.ac.uk/red/research-policy/pure/user-guides/ebr-terms/

Dynamical Systems: An International Journal
Vol. 00, No. 00, July 2004, 1–25

Periodic solutions and their bifurcations in a non-smooth second-order delay differential equation

DAVID A. W. BARTON*, BERND KRAUSKOPF, and R. EDDIE WILSON

Bristol Centre for Applied Nonlinear Mathematics, University of Bristol,
Queen's Building, Bristol BS8 1TR, United Kingdom

(Submitted June 2005)

We consider a non-smooth second order delay differential equation (DDE) that was previously studied as a model of the pupil light reflex. It can also be viewed as a prototype model for a system operated under delayed relay control.

We use the explicit construction of solutions of the non-smooth DDE hand-in-hand with a numerical continuation study of a related smoothed system. This allows us to produce a comprehensive global picture of the dynamics and bifurcations, which extends and completes previous results. Specifically, we find a rich combinatorial structure consisting of solution branches connected at resonance points. All new solutions of the smoothed system were subsequently constructed as solutions of the non-smooth system. Furthermore, we show an example of the unfolding in the smoothed system of a non-smooth bifurcation point, from which infinitely many solution branches emanate. This shows that smoothing of the DDE may provide insight even into bifurcations that can only occur in non-smooth systems.

1 Introduction

In recent years there has been much interest in non-smooth equations from a variety of perspectives. Applications of non-smooth equations include mechanical systems involving impacts [6] or frictional forces [22], electrical systems with switching effects [3], and biological systems with threshold or saturation effects [13]. We focus here on piecewise smooth models, which are particularly useful for modelling systems that can be represented by a combination of different vector fields. In an abstract setting, piecewise smooth models partition phase space into disjoint regions with distinct dynamics; see [8, 18, 26, 27] as general references. In many cases the dynamics in each region is simpler than the equivalent smooth system, and the main issue is then to find or construct solutions of the system from individual solution segments in each region.

*Email: david.barton.99@bristol.ac.uk

In this paper we consider non-smooth delay differential equations (DDEs) where there is a constant time delay τ in the system response. Such a delay arises naturally in many applications including the reaction time of a human observer [7], actuation delays [16], sampling delays [17], and communication delays [20]. Non-smooth DDEs arise directly from a range of different applications including delayed relay control [4,11,12,15,24], discrete sampling in a control system [17], delayed linear control with saturation effects [21], and the pupil light reflex [1,2,5].

Delay differential equations define a dynamical system with an infinite dimensional phase-space [14] because the history over the delay interval $[-\tau, 0]$ must be specified as the initial condition. Due to this infinite dimensionality DDEs are difficult to analyse analytically and much is still unknown about their dynamics [9,14,25]. However the combination of delay and non-smoothness allows us to study high-dimensional dynamics in an apparently simple equation.

The specific model we investigate is the non-smooth DDE

$$\begin{aligned} \dot{x}(t) &= y(t) \\ \dot{y}(t) &= -x(t) - \begin{cases} -\frac{1}{2} & \text{if } x(t-\tau) < \Theta, \\ +\frac{1}{2} & \text{if } x(t-\tau) \geq \Theta. \end{cases} \end{aligned} \tag{1}$$

where $\tau > 0$ is the fixed delay, and Θ is a constant switching threshold. Equation (1) has previously been studied by an der Heiden *et al.* [1], an der Heiden and Reichard [2], and Bayer and an der Heiden [5] as a non-dimensionalised model of the pupil light reflex [19]. Additionally (1) can be viewed as a prototype equation for a system operated under relay control where a controller switches a system between two discrete states, e.g., on or off ("bang-bang" control); for examples see [11,12,23,24].

Equation (1) has reflectional symmetries in the x and y variables (see (4) and (5)), and different families of solutions may be defined according to which of these symmetries they possess. Periodic solutions of (1) can be constructed explicitly by piecing together individual solution segments with suitable boundary conditions. Specifically, all periodic solutions of (1) consist of sequences of circular arcs in the (x, y) plane that are centred about one of two rotation centres at $(x = \pm\frac{1}{2}, y = 0)$. This construction is applied in [1,5] to find families of simple periodic solutions (with exactly two discontinuities in $\dot{y}$ per period), and their domains of existence in the (τ, Θ) parameter plane. However, a detailed bifurcation study has not been performed.

In this paper we present a comprehensive picture of the dynamics and bifurcations of (1), which extends and completes the work of an der Heiden *et al.* [1,5]. To this end we use two technical tools hand-in-hand: the explicit con-

struction of solutions in the non-smooth system and numerical continuation in the related smoothed system

$$\begin{aligned} \dot{x}(t) &= y(t), \\ \dot{y}(t) &= -x(t) - \tfrac{1}{2}\tanh\left(\frac{\Theta - x(t-\tau)}{\varepsilon}\right), \end{aligned} \tag{2}$$

which retains the symmetries of the original non-smooth DDE (1). Here the parameter ε determines the degree of smoothing, and must be chosen sufficiently small to ensure that the solutions of (2) are close to those of (1). On the other hand, ε must be large enough for numerical continuation to be computationally tractable. Throughout this paper we fix $\varepsilon = 0.01$.

The explicit construction of many new families of periodic solutions with multiple discontinuities per period is guided by numerical bifurcation analysis. For this purpose we use the software DDE-BIFTOOL [10] — a Matlab package for the numerical continuation of solutions (both equilibria and periodic solutions) of delay differential equations (with multiple fixed or state dependant delays). In addition DDE-BIFTOOL has the facility to calculate the Floquet multipliers of a periodic solution. This permits the detection and classification of all the bifurcations present, which is very difficult when using solution constructions alone.

The dynamics of (2) are organised by a sequence of resonance points that lie on two families of solution branches (with two discontinuities in $\dot{y}$ per period). Bifurcating branches of more complicated types of solutions connect different resonance points in an interesting combinatorial structure. Our bifurcation analysis reveals the parts of solution branches that are stable. We checked by explicit construction that the solutions in (2) indeed have their counterparts in the non-smooth system (1). In particular, we found that a non-smooth bifurcation point, which cannot occur in the smoothed system, has a counterpart in (2) in the form of a 'fan' of infinitely many bifurcation points, from which the corresponding solution branches bifurcate. As the smoothing parameter is decreased we observe that the non-smooth bifurcation is approached in a definite way.

The outline of the paper is as follows. In section 2 we explain the construction of solutions of (1) and summarise the previous results. In section 3 we use constructed solutions as starting data for their numerical continuation as solutions of the smoothed system (2). How resonance points organise the different branches of solutions is investigated in section 4. We conclude and provide an outlook to future research in section 5.

2 Notation and background material

In this section we introduce the notation used throughout the paper and describe the construction of non-smooth solutions. We then summarise the previous results for the non-smooth system (1) from [1, 2, 5].

2.1 *Construction of solutions*

We define the *switching line* of both the non-smooth system (1) and the smoothed system (2) as the line $x = \Theta$. Time τ after the solution passes through this switching line a *switch* occurs in the solution; this corresponds to a discontinuous change in the vector field of (1) and a zero in the tanh nonlinearity of (2). The *switching points* (x, y) and *switching times* (t) of a solution are defined as the locations and times, respectively, where switches occur. Additionally the current *switch state* is given by the sign of the nonlinearities in (1) and (2).

A unique solution of the non-smooth system (1) is determined by a suitable *initial condition* namely a segment of solution of time τ in length. The initial condition can be written as an initial point $(x(0), y(0))$ along with an initial sequence of switching times $\{t_1, t_2, \ldots, t_n\}$ such that $0 \leq t_n \leq \tau$ and an initial switch state (i.e., the sign of the non-smooth term at $t = 0$). Without loss of generality we assume throughout that $t_1 = 0$ (which can be achieved by a time shift).

The solutions of (1) are composed of a sequence of circular arcs that are centred about $(\pm 1/2, 0)$. Assuming that the initial switch state is negative, these arcs are determined by the initial conditions and are given by

$$\begin{aligned} x(t) &= \tfrac{1}{2}(-1)^i + A_i \sin(t + \phi_i), \\ y(t) &= A_i \cos(t + \phi_i), \\ t &\in [t_i, t_{i+1}]. \end{aligned} \tag{3}$$

The requirement that the solution is continuous for all time fixes values for A_i and ϕ_i. Subsequent switching times $t_{n+i} \geq \tau$ for $i \in \mathbb{N}$ are determined by the solution crossing the switching line $x = \Theta$ time τ earlier.

Throughout this paper we consider periodic solutions of (1) and (2), namely solutions that possess the property that $(x(t + T), y(t + T)) = (x(t), y(t))$ where T is the (minimal) period of the solution. In order to find periodic solutions we must obtain values for $x(0)$, $y(0)$ and t_i such that the periodicity condition is satisfied. To do this directly requires solving a system of nonlinear algebraic equations that are also non-smooth at the switching points. This is the approach of an der Heiden *et al.* [1] and Bayer and an der Heiden [5] for

the simplest case where the periodic solutions have two switching points per period.

2.2 *Types of periodic solutions*

As was mentioned systems (1) and (2) have the two reflectional symmetries

$$\mathrm{R}_x : (x,t) \to (-x,-t) \quad \text{for } \Theta = 0, \tag{4}$$

$$\mathrm{R}_y : (y,t) \to (-y,-t) \quad \text{for all } \Theta. \tag{5}$$

Following the notation set out in [1, 2] we divide the solutions of (1) and (2) into four types according to which of these reflectional symmetries they possess:

L *Lens* solutions possess the symmetry R_y and for $\Theta = 0$ the additional symmetry R_x. They have a period of $T = \tau$ with two switching points per period on the line $x = \Theta$. An example of a lens solution is shown in fig. 1(a).

G *Glasses* solutions possess the symmetries R_x and R_y. They have a period of $T = 2\tau$ with two switching points per period on the line $x = \Theta$. An example of a glasses solution is shown in fig. 1(b).

P *Potato* solutions possess the symmetry R_y. They have a period of $T = 2\tau$ with any (even) number of switching points per period. An example of a potato solution is shown in fig. 1(c). More complex potato solutions consist of arcs that encircle the points $(\pm 1/2, 0)$ multiple times.

H *Heart* solutions possess the symmetry R_x for $\Theta = 0$ and for non-zero values of Θ they have no symmetries. They have a period of $T = 2\tau$ and any (even) number of switching points per period. An example of a heart solution is shown in fig. 1(d). More complex heart solutions consist of arcs that encircle the points $(\pm 1/2, 0)$ multiple times.

The left-hand column of fig. 1 shows the phase-plane projections of examples of the different solution types for $\Theta = 0$ and the right-hand column shows the time-plots of the examples. In both columns the switching points and switching times are numbered.

Throughout this paper we label branches of a particular solution type with the letters as introduced above. A subscript is used to distinguish between distinct branches of the same type.

Note that glasses solutions do not exist for non-zero values of Θ as the symmetry R_x is broken. In general glasses solutions are a sub-type of potato solutions. We distinguish glasses solutions from potato solutions because of the importance of this sub-type, as is shown in section 4.

Due to the symmetries present in both (1) and (2), all potato solutions (for $\Theta = 0$) and heart solutions (for all values of Θ) exist as asymmetric pairs. The asymmetric counterpart of a potato solution can be found by the application of the symmetry R_x and, similarly, the asymmetric counterpart of a heart solution can be found by the application of the symmetry R_y. We denote the asymmetric counterpart of a particular solution by a superscript asterisk, e.g., P_1 and P_1^* are an asymmetric pair.

The existence of lens, glasses and potato solutions is proved by constructive methods in [1] for $\Theta = 0$ and in [5] for $\Theta \neq 0$. The existence of heart solutions is mentioned in [2] but no details are given regarding their construction.

If there exists a periodic solution of (1) or (2) for $\tau = \tau_1 < T$ where T is the period of the solution, then there exist infinitely many *secondary solutions* with

$$\tau = \tau_n = \tau_1 + (n-1)T \qquad n \in \mathbb{N}. \tag{6}$$

This means that the delay τ in the delayed term $x(t-\tau)$ can be reduced modulo the period of the solution. This arises directly from the definition of a periodic solution, that is, $x(t+T) = x(t)$ for all t. The time series of the secondary solutions are identical and, consequently, their projections in phase space are also identical. Although the secondary solutions have identical time series, due to the change in the time-delay τ, the Floquet multipliers of the solutions are different.

We use (6) to define the *primary solution branches* as the branches of solutions for which the time delay is minimal, i.e., $\tau < T$ for all solutions along the branches. The *secondary solution branches* are all the branches of solutions where the time delay is not minimal, i.e., $\tau > T$ for all solutions along the branches. Since the Floquet multipliers of each of the secondary solutions are different from each other, the bifurcations that occur on each secondary branch are also different. Throughout this paper we use a superscript to distinguish between the (secondary) branches. The superscript is given by the value of n in (6).

2.3 *Previous work*

We now summarise the work by an der Heiden *et al.* [1] and Bayer and an der Heiden [5] on the periodic solutions of (1). They constructed the primary branches of lens and glasses solutions for the non-smooth system (1) and also a single primary branch of potato solutions. These are constructed for $\Theta = 0$ in [1] and for $\Theta \neq 0$ in [5]; see [5, figs. 6 and 7] for graphical representations. Additionally, in [5] the stability of the primary branches of constructed solutions is determined analytically. The stability of the secondary branches is

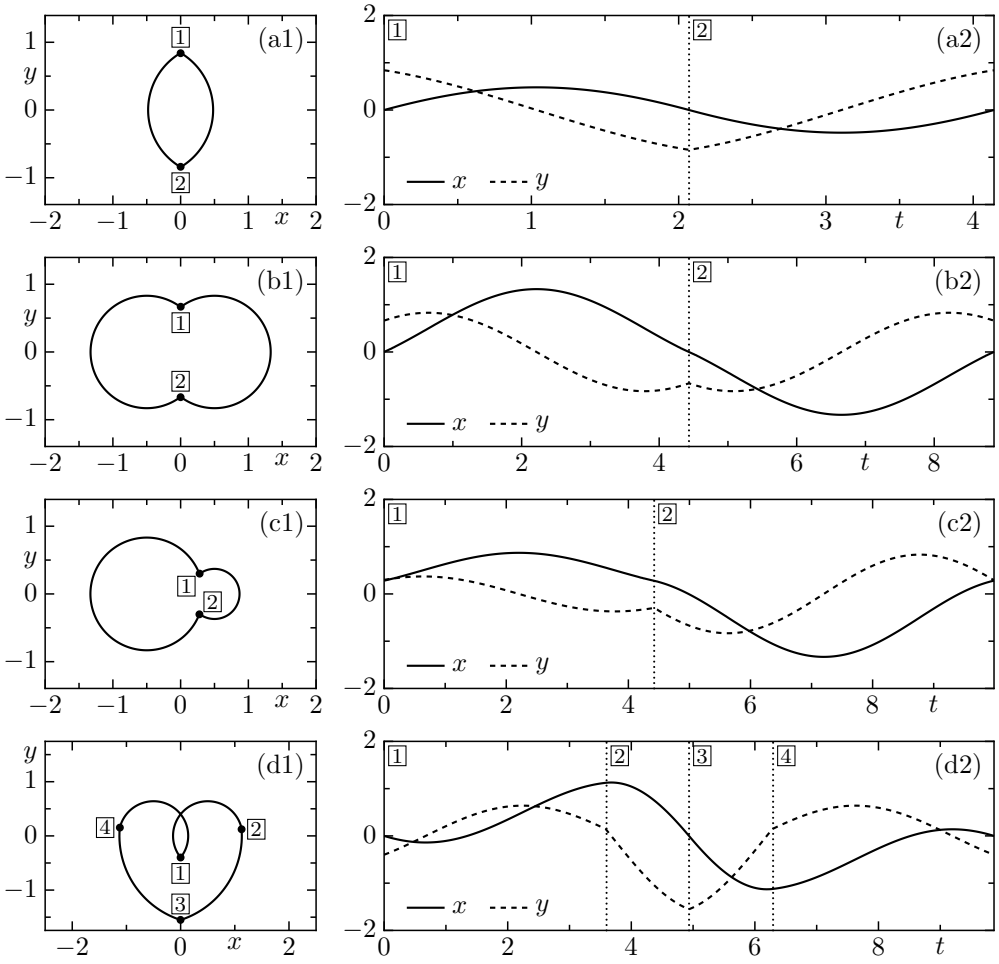

Figure 1. Examples of the four different types of periodic solution of (2) for $\Theta = 0$. The phase portraits of the different solutions are shown on the left column and their time series in the right column. The numbered lines and points correspond to the switches in the solution. ($\tau = 4.14$, 4.43, 4.99 and 4.94 respectively.)

determined by numerical simulation only. We show in fig. 2 the branches of smoothed solutions of (2) that correspond to the branches of solutions constructed in [1, 5] for $\Theta = 0$ and $\Theta = 0.1$. We plot the continuation parameter τ against the solution norm $\|y\|$ which is defined as

$$\|y\| := \max y(t) - \min y(t). \tag{7}$$

This norm allows us to distinguish between different branches; almost all branch crossings in the $(\tau, \|y\|)$-plane are bifurcations. However it should be

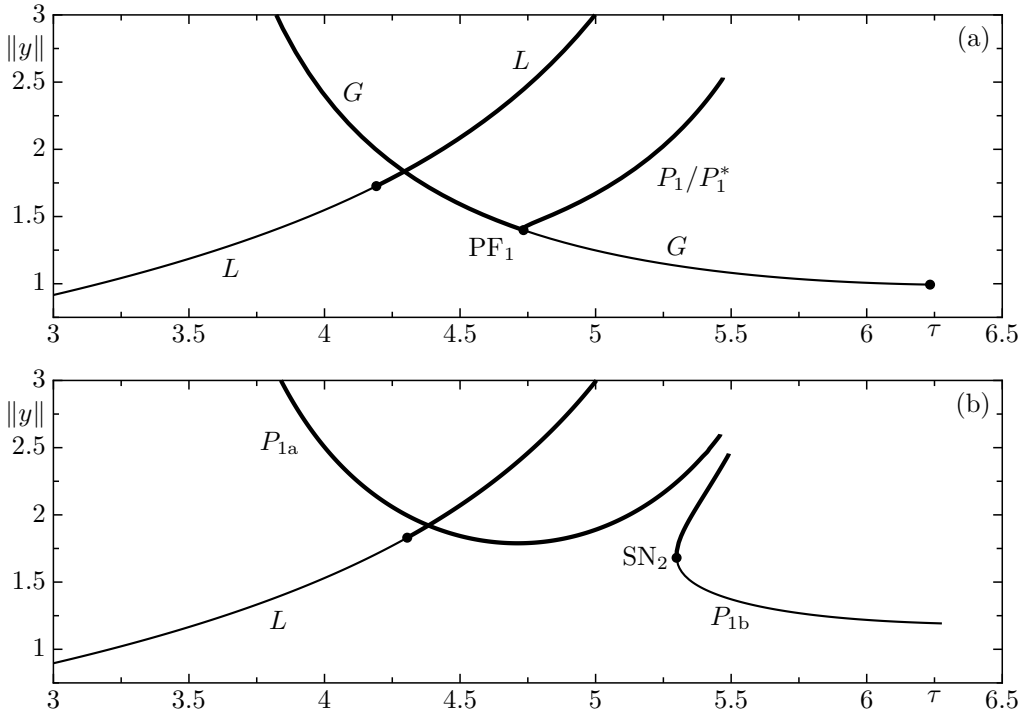

Figure 2. The primary branches of periodic solutions of (1) as described in [1] for $\Theta = 0$ and in [5] for $\Theta \neq 0$ are reproduced here for the smoothed system (2) where the continuation parameter τ is plotted against the solution norm $\|y\|$. The branch segments that are in bold denote stable solutions; all other solutions are unstable. Panels (a) and (b) show the branches for $\Theta = 0$ and $\Theta = 0.1$ respectively.

noted that in fig. 2(a) the crossing of the branch of lens solutions L with the branch of glasses solutions G is the result of projection (7) rather than the occurrence of a bifurcation. Similarly the crossing of L and P_{1a} in fig. 2(b) is not a bifurcation. To distinguish between bifurcations and crossings due to the projection we mark all bifurcation points with dots.

We now describe the results from [1] for $\Theta = 0$, as reproduced in fig. 2(a). The bifurcations shown here and in later figures are labelled as follows: saddle-node bifurcation (SN); pitchfork bifurcation (PF); period doubling bifurcation (PD); resonance point (RS); cusp point (CU). Subscripts are used to distinguish between different bifurcations of the same type.

The branch G of glasses solutions exists in the parameter region $\pi < \tau < 2\pi$. For glasses solutions (fig. 1(b)) the angle swept out by the solution arc between consecutive switching points is equal to τ. Consequently as τ tends to π the solution norm $\|y\|$ tends to ∞. Similarly as τ tends to 2π the solution norm $\|y\|$ tends to 1. Figure 2(a) shows that G loses stability at the pitchfork bifurcation PF_1. Two branches of asymmetric potato solutions P_1 and P_1^*

begin at PF_1; these are asymmetric counterparts as described in section 2.1. Because solutions on P_1 and P_1^* have the same norm (7), the branches are projected on top of each other. The branch of lens solutions L exists in the parameter region $0 < \tau < 2\pi$. The angle swept out by the solution arc between consecutive switching points is equal to $\tau/2$ (see fig. 1(a)). Thus $\|y\| \to 0$ as $\tau \to 0$ and $\|y\| \to \infty$ as $\tau \to 2\pi$.

Figure 2(b) reproduces the results obtained in [5] for $\Theta = 0.1$. In this case the reflectional symmetry about $x = 0$ of (1) and (2) is broken. Thus the branches of potato solutions P_1 and P_1^* no longer exist as an asymmetric pair. The pitchfork bifurcation PF_1 for $\Theta = 0$ is unfolded into the saddle-node bifurcation SN_2. Consequently, the branch of glasses solutions G is now split in two and together with the branches P_1 and P_1^* forms part of the new branches $P_{1\mathrm{a}}$ and $P_{1\mathrm{b}}$. All branches shown in fig. 2(b) are constructed in [5] for $|\Theta| < 0.5$. However, no global picture of the dynamics is given. The branches G and P_1 shown in fig. 2(a) appear to end without reason (similarly branches $P_{1\mathrm{a}}$ and $P_{1\mathrm{b}}$ in fig. 2(b)); this suggests that there are branches of yet unknown solutions and additional bifurcations to be found. Particularly the bifurcation that occurs at the change of stability in L is not classified in [1, 5].

3 The primary branches

Comparing the results of [1] and [5] to the results of the numerical continuations shown in fig. 2 we see that using the smoothed system (2) gives a good approximation to the non-smooth system (1). In what follows we perform a bifurcation analysis of the smoothed system (2) to come to a comprehensive global picture of the dynamics of the non-smooth system (1).

3.1 *Complete bifurcation diagram for* $\Theta = 0$

Figure 3(a) shows completed bifurcation diagram for (2); notice the additional solution branches and bifurcations in addition to from those shown in fig. 2(a). Specifically, an unstable branch of potato solutions P_2 bifurcates from SN_1. The solutions on P_2 all have four switching points per period; fig. 3(b) is an example of such a solution. The branch P_2 ends at the 1:2 resonance point $\mathrm{RS}_{1:2}$ on the branch of lens solutions L; at this point the period of the potato solutions is twice that of the lens solutions. This resonance point is characterised by a pair of Floquet multipliers passing through the unit disc at -1.

From the resonance point $\mathrm{RS}_{1:2}$ two branches of heart solutions H_1 and H_1^* bifurcate. Two of the solutions along H_1 are shown in figs. 3(c) and (d). All these heart solutions have four switching points per period. The two branches H_1 and H_1^* terminate at the pitchfork bifurcation PF_2 on the branch of glasses

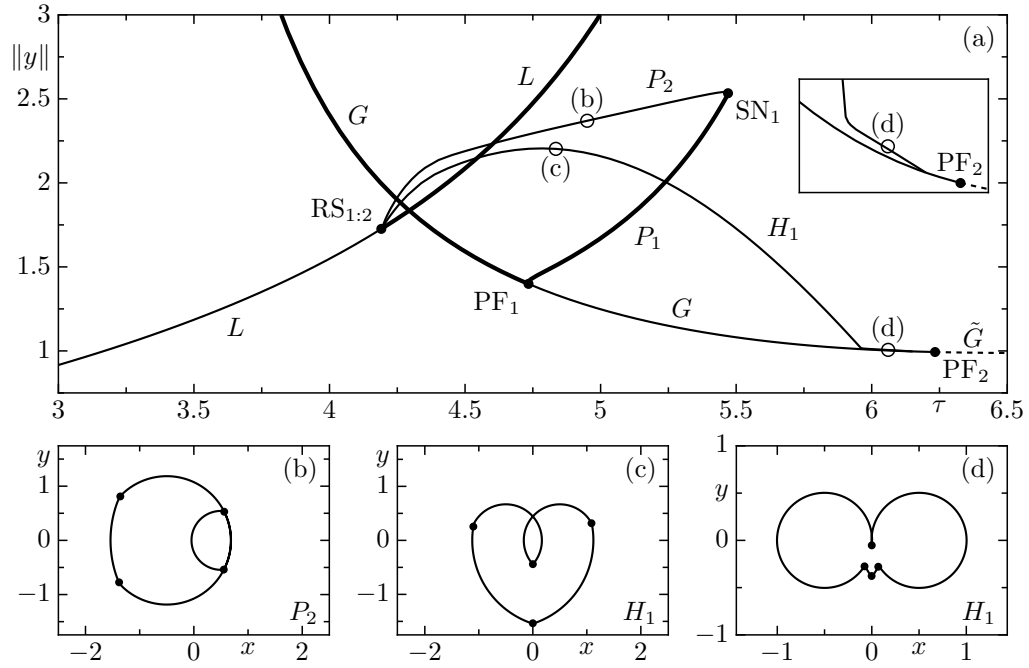

Figure 3. Panel (a) shows the completed bifurcation diagram of (2) (cf., fig. 2(a)). Panels (b), (c) and (d) are phase-portraits of different solution types each with four switching points per period whose locations are also labelled in panel (a). Panel (b) shows a potato solution and panels (c) and (d) show heart solutions. The asymmetric counterpart to the heart solutions are given by a reflection about $y = 0$.

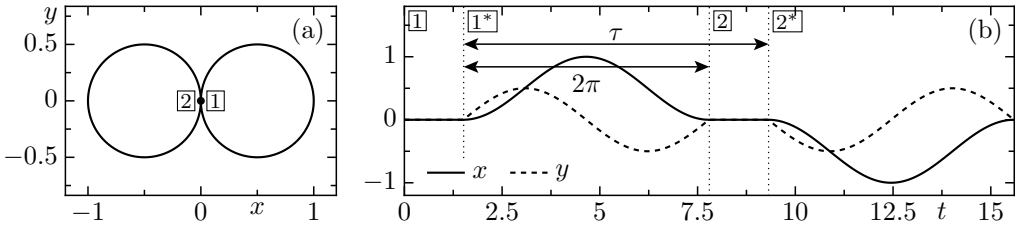

Figure 4. A glasses solution in the branch G for $\tau = 7.8$ that exists in the smoothed system (2) but not in the non-smooth system (1). Panel (a) shows the phase-plane projection and panel (b) shows the time series for one period. The solution spends time $\tau - 2\pi$ on the switching line at switching points 1 and 2 before moving off.

solutions G. As the branches approach PF_2 they become very close to the branch G in the norm (7). The extra switches of the heart solution contribute very little to the norm as can be seen from fig. 3(d).

The branch G continues through the pitchfork bifurcation PF_2 at $\tau = \tau' \approx 2\pi$ and exists for arbitrarily large values of τ. This branch is marked by a dashed line in fig. 3(a) and labelled $\tilde{G}$. Whereas the solutions on G that exist

for $\tau < \tau'$ pass through the switching line $x = 0$ instantaneously, the solutions that exist for $\tau > \tau'$ spend approximately time $2\pi - \tau$ in the immediate neighbourhood of the switching line before moving away. A solution for $\tau > \tau'$ is shown in fig. 4. The phase-portraits of all the glasses solutions for $\tau > \tau'$ are very similar; only the amount of time spent close to the switching line changes.

We now consider how the results from the continuation of the smoothed system (2) relate to the non-smooth system (1). First we ensure that the smoothed solutions found are solutions of (1) when the smoothing is taken to the limit $\varepsilon \to 0$. That is we show that the new potato and heart solutions exist for (1). We use the solution construction (3) to give the following algebraic system

$$\begin{aligned}
\tfrac{1}{2} + A_1 \sin(t_1 + \phi_1) &= -\tfrac{1}{2} + A_2 \sin(t_1 + \phi_2),\\
-\tfrac{1}{2} + A_2 \sin(t_2 + \phi_2) &= \tfrac{1}{2} + A_3 \sin(t_2 + \phi_3),\\
\tfrac{1}{2} + A_3 \sin(t_3 + \phi_3) &= -\tfrac{1}{2} + A_4 \sin(t_3 + \phi_4),\\
-\tfrac{1}{2} + A_4 \sin(t_4 + \phi_4) &= \tfrac{1}{2} + A_1 \sin(\phi_1),\\
A_1 \cos(t_1 + \phi_1) &= A_2 \cos(t_1 + \phi_2),\\
A_2 \cos(t_2 + \phi_2) &= A_3 \cos(t_2 + \phi_3),\\
A_3 \cos(t_3 + \phi_3) &= A_4 \cos(t_3 + \phi_4),\\
A_4 \cos(t_4 + \phi_4) &= A_1 \cos(\phi_1),\\
x(t_1 - \tau) &= \Theta,\\
x(t_2 - \tau) &= \Theta,\\
x(t_3 - \tau) &= \Theta,\\
x(t_4 - \tau) &= \Theta,
\end{aligned} \tag{8}$$

where

$$x(t) = \begin{cases} A_1 \sin(t + \phi_1) & \text{if } \ 0 \le t < t_1,\\ A_2 \sin(t + \phi_2) & \text{if } \ t_1 \le t < t_2,\\ A_3 \sin(t + \phi_3) & \text{if } \ t_2 \le t < t_3,\\ A_4 \sin(t + \phi_4) & \text{if } \ t_3 \le t < t_4 \end{cases} \tag{9}$$

with periodic extension. Equations (8) and (9) are necessary conditions (but not sufficient) for the existence of a periodic solution with four switching points per period. They ensure that the solution is continuous in x and y and also that the switching points occur time τ after the solution crosses the switching

line. For completeness (or implication both ways) we must add the following sufficiency conditions:

(i) $x(t) = \Theta$ has only four roots per period.
(ii) The sign of $x(t-\tau)-\Theta$ is consistent with the vector field (1) for $0 \leq t \leq t_4$.

From the smoothed solutions produced by DDE-BIFTOOL we find approximate values for the constants (A_i, ϕ_i, t_i). These approximate values are then entered into a Newton iteration solver for (8) and (9). Once the Newton iteration has converged we check that the additional sufficiency conditions above hold, in which case we find a solution of (1) as $\varepsilon \to 0$.

The Newton iterations converge when started close to the solutions on P_2 and H_1. In this way we checked that all the new solutions of (2) in fig. 3 indeed exist as solutions of the non-smooth system (1). As SN_1 is approached on P_2 the switching points of the solutions on the branch come together. Consequently in (1) a grazing bifurcation [8,26] occurs at the end of the branch P_2, simultaneously with SN_2. It is at this grazing bifurcation that the number of switching points per period of the solutions changes from two per period on P_1 to four per period on P_2.

In contrast to the branches P_2 and H_1 we find that the branch of glasses solutions starting at PF_2 and labelled $\tilde{G}$ (shown by a dashed line in fig. 3) does not exist in the non-smooth limit. Instead the branch G terminates at PF_2. This suggests that an additional non-smooth bifurcation occurs simultaneously with PF_2. In section 4.3 we show how this non-smooth bifurcation unfolds when (1) is smoothed to become (2).

3.2 *Complete bifurcation diagram for* $\Theta \neq 0$

We now consider the case of non-zero Θ; this corresponds to breaking the reflectional symmetry R_x of (1) and (2). Similar to the case for $\Theta = 0$, fig. 5(c) shows the extra bifurcations and branches missing from fig. 2(b).

Figure 5(a) shows a two-parameter bifurcation diagram in the (τ, Θ)-plane. It is built from 45 individual one-parameter continuations with a change in Θ of 0.025 between each continuation. This scripting is necessary because as yet it is not possible to continue bifurcations of periodic solutions in two parameters with DDE-BIFTOOL. Additional one-parameter continuations were performed close to $\Theta = 0$ to ensure that any fine detail was captured. Three representative one-parameter continuations are shown in figs. 5(b)–(d) for $\Theta = 0.05$, 0.1 and 0.3, respectively. They should be compared with fig. 2(a) for $\Theta = 0$.

The two-parameter bifurcation diagram provides a global picture of the bifurcations that occur in the smoothed system (2). Each of the regions marked in fig. 5(a) corresponds to different parameter regimes that have a particular set of coexisting solutions. Figure 5(a) shows how the bifurcations that

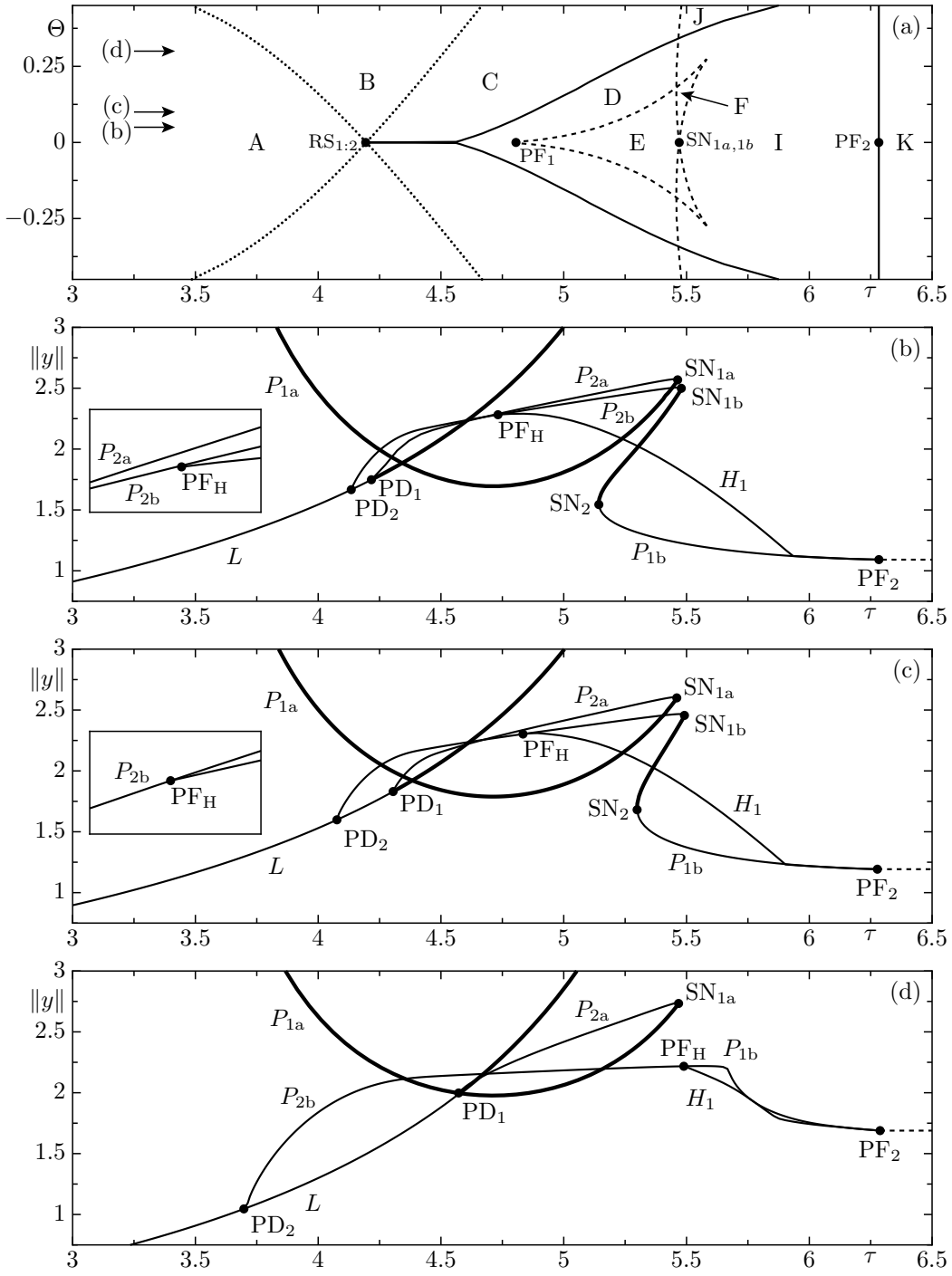

Figure 5. Panel (a) shows the two-parameter bifurcation diagram in the (τ, Θ)-plane. The solid lines are pitchfork bifurcations, the dotted lines are period-doubling bifurcations, and the dashed lines are saddle-node bifurcations. The bifurcations for $\Theta = 0$ are labelled (cf. fig. 3). Panels (b), (c) and (d) are one-parameter continuations in τ for $\Theta = 0.05$, 0.1 and 0.3, respectively.

Region	Stable solutions	Unstable solutions
A	P_{1a} ($\tau > \pi$)	L
B	P_{1a}	L, P_{2b}
C	L, P_{1a}	P_{2a}, P_{2b}
D	L, P_{1a}	P_{2a}, P_{2b}, H_1, H_1^*
E	L, P_{1a}, P_{1b}	P_{1b}, P_{2a}, P_{2b}, H_1, H_1^*
F	L, P_{1b}	P_{1b}, P_{2b}, H_1, H_1^*
I	L	P_{1b}, H_1, H_1^*
J	L	P_{2b}
K	-	-

Table 1. The stable and unstable solutions existing in the different regions of the two-parameter bifurcation diagram shown in fig. 5.

exist for $\Theta = 0$ unfold. In particular the pitchfork bifurcation PF_1 unfolds into saddle-node bifurcations, and the resonance point $\mathrm{RS}_{1:2}$ unfolds into two period-doubling bifurcations and a pitchfork bifurcation. (Pitchfork bifurcations can continue to exist for non-zero Θ since there remains the reflectional symmetry R_y.) Additionally we see that two cusp bifurcations occur at approximately $\Theta = \pm 0.27$, $\tau = 5.58$.

Figures 5(b)–(d) are three one-parameter bifurcation diagrams for different values of Θ. Figures 5(b) and (c) illustrate how the case $\Theta = 0$ is unfolded (cf., fig. 3). Figures 5(b) and (c) are topologically equivalent but show how this transition increasing manifests itself. The branch of heart solutions H_1 no longer bifurcates from the branch of lens solutions L, but instead it bifurcates from the branch of potato solutions P_{2b} at the pitchfork bifurcation PF_H. Figure 5(d) shows a one-parameter continuation for $\Theta = 0.3$ that is topologically different from figs. 5(b) and (c) as the two branches of saddle-node bifurcations have terminated at a cusp bifurcation. Consequently the branch P_{1b} is now entirely unstable.

Figure 5 completes the partial bifurcation diagrams of an der Heiden *et al.* [1] and Bayer and an der Heiden [5] shown in fig. 2 for $\Theta = 0$ and $\Theta \neq 0$. The different parameter regimes as marked on fig. 5(a) are summarised in tab. 1.

Similar to the case for $\Theta = 0$ it is possible to construct the solutions found using DDE-BIFTOOL for the non-smooth system (1) using the algebraic system (8). Again the glasses solutions after the pitchfork bifurcation PF_2 do not exist in the non-smooth limit (indicated by the dashed line on figs. 5(b)–(d)).

4 Bifurcations of the secondary branches

In this section we focus on the secondary branches of glasses and lens solutions. For a particular value of the norm the solutions in each secondary branch have identical time series and phase-plane projections. However, the time delay τ changes according to (6), which causes the Floquet multipliers of the solutions to vary from branch to branch. These secondary branches are constructed but not studied in [1, 2, 5]. We use DDE-BIFTOOL to show that new branches bifurcating from secondary branches are important for understanding the non-smooth bifurcations of (1). Finally we combine all our results to give a comprehensive overview of the bifurcation structure of the non-smooth system (1).

The resonance points along each of the secondary branches of lens solutions are divided into two groups. Note that any resonance p:q may also be written as $(q-p)$:q. For purposes of comparison we fix the resonances as they are written in fig. 6. If a resonance p:$q < 1$:2, i.e., $\frac{p}{q} < \frac{1}{2}$, there exist multiple branches of complicated potato and heart solutions that connect the resonance point to another resonance point on a branch of glasses solutions. On the other hand if a resonance p:$q \geq 1$:2, i.e., $\frac{p}{q} \geq \frac{1}{2}$, the branches starting at the resonance point instead end at a pitchfork bifurcation on $\tilde{G}$; it is these branches that show how the non-smooth bifurcations of (1) are unfolded.

4.1 *Secondary branches of glasses and lens solutions*

Figure 6 shows the branches of glasses and lens solutions. The branches G and L are the primary branches and the branches G^i and L^i for $i \in \{2, 3, \ldots\}$ are the secondary branches as given by (6). The bifurcations along these branches are either pitchfork bifurcations (labelled PF) or resonance points with resonances as shown in the figure.

The branches that bifurcate from the primary branches G and L (e.g., P_1 and H_1) are also repeated according to (6). Thus, without calculating the Floquet multipliers along the secondary branches of glasses and lens solutions, we already know the parameter values for which particular bifurcations exist. For example, each repeated branch of glasses solutions must have two pitchfork bifurcations at prescribed values of τ, simply because the primary branch G possesses two pitchfork bifurcations. Similarly, the resonance point $\mathrm{RS}_{1:2}$ on the primary branch of lens solutions L must also be repeated, although they repeat on only every second branch (i.e., L^3, L^5, etc.) because the branches bifurcating from $\mathrm{RS}_{1:2}$ have a period twice that of the solutions on L. For both lens and glasses solutions each secondary branch has one more resonance point than the previous secondary branch.

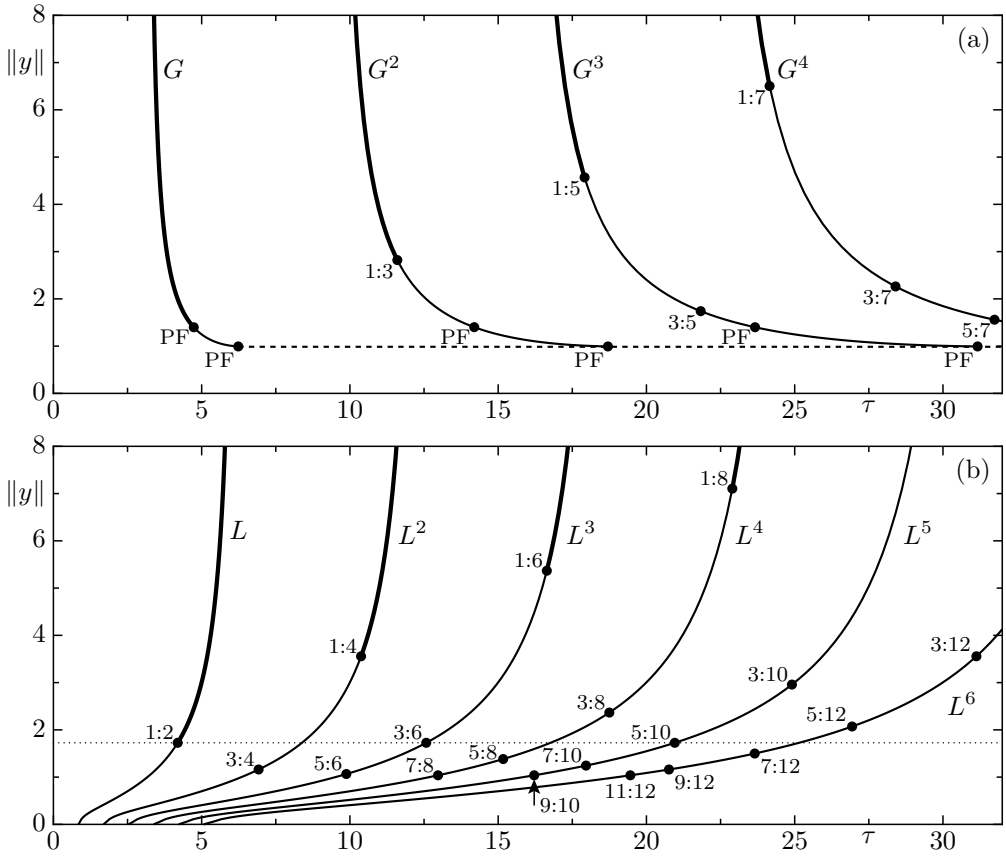

Figure 6. Panel (a) shows the primary branch of glasses solutions G along with three secondary branches. Panel (b) shows the primary branch of lens solutions L along with five secondary branches. Bold curves indicate stable solutions; all other branches are unstable. PF denotes a pitchfork bifurcation and all other bifurcations are Neimark-Sacker bifurcations with resonances as shown.

These secondary branch resonances together with further numerical observations show that there is an interesting combinatorial structure to the resonances. Additionally the resonances of (2) appear to follow a strict pattern. On the branch of glasses solutions G^i we observe the resonance points

$$\mathrm{res}_G(i) = \{(2j-1)/(2i-1) : j \in \mathbb{N} < i\}.$$

Whereas on the branch of lens solutions L^i we observe the resonance points

$$\mathrm{res}_L(i) = \{(2j-1)/(2i) : j \in \mathbb{N} \leq i\}.$$

In the following sections we investigate the branches that bifurcate from these

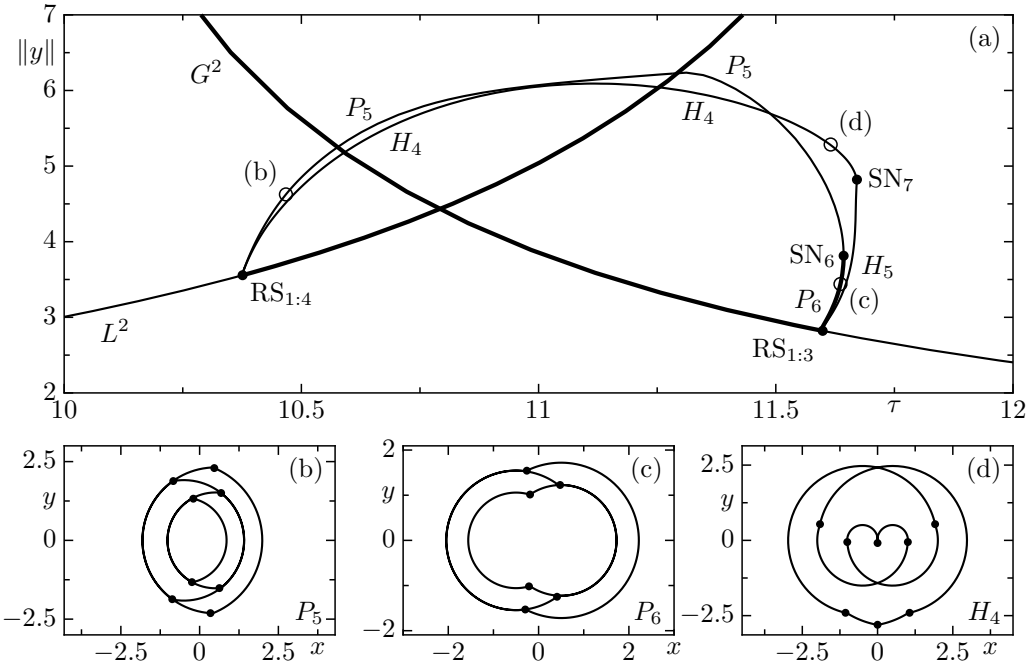

Figure 7. Panel (a) shows the branches of solutions that bridge two resonance points $RS_{1:4}$ and $RS_{1:3}$ respectively. Two branches of potato solutions and two branches of heart solutions bifurcate from each resonance point. Panels (b), (c) and (d) are examples of solutions at points along the branches.

resonance points with DDE-BIFTOOL and we find an interesting connecting structure between the resonance points on different secondary branches.

4.2 *Branches that bridge the resonance points*

Figure 7(a) shows four branches of periodic solutions ($P_{5,6}$ and $H_{4,5}$) that bridge the two resonance points $RS_{1:4}$ on L^2 and $RS_{1:3}$ on G^2. Numerical investigations of other secondary branches indicate that the resonance points on branches of lens solutions with resonances $p{:}q < 1{:}2$ are connected to a resonance point on a branch of glasses solutions in the same way as shown in fig. 7(a). Hence fig. 7(a) represents a generic scenario.

At $RS_{1:4}$ the branch L^2 gains stability and four branches bifurcate off (P_5, P_5^*, H_4, and H_4^*). The solutions on the bifurcating branches are significantly more complex than solutions previously seen, as is shown in fig. 7(b)–(d). They have eight switching points per period and their phase-plane projection shows that the solution arcs may overlay each other. Figure 8 shows a phase-plane projection of a more complex solution alongside its time-plot with each of the switching points numbered. Each of the branches in fig. 7(a) then undergoes

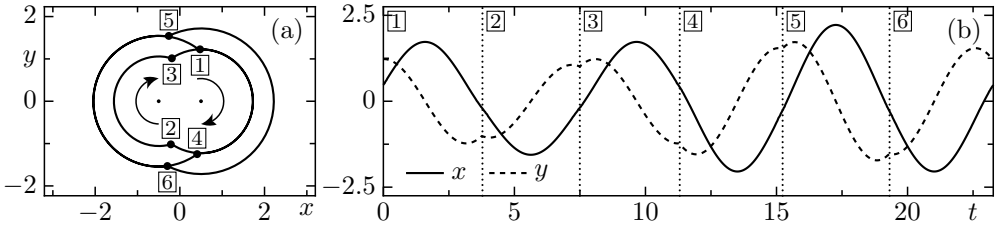

Figure 8. A potato solution with six switching points per period. Panel (a) shows a phase-portrait of this solution and panel (b) shows a time-plots of this solution. The numbered points are the switching points in the solution.

a saddle-node bifurcation. The stability of the branches of heart solutions remains unchanged at SN_7, however the branches of potato solutions gain stability at SN_6. Thus there is a region in parameter space where there are three stable solutions; on P_6, P_6^* and L^2. Close to $RS_{1:3}$ the solutions on P_6 and H_5 have six switching points per period. Thus in the non-smooth system (1) there must be an additional grazing bifurcation on each of the bridging branches.

We extend (8) and (9) to consider non-smooth solutions of (1) with six and then with eight switching points per period. This produces algebraic systems of 18 and 24 equations, respectively. We used the smoothed solutions as starting data for a Newton iteration to find the corresponding exact solutions of (1). In this manner the existence of these solutions in the non-smooth limit of (2) was confirmed. In general, the number of switching points per period of solutions on the bridging branches have is determined by the resonance of the point from which they bifurcate. For a resonance p:q the bifurcating branches have $2q$ switching points per period.

4.3 *Resonance points with p:q > 1:2*

Figure 9(a) shows the four branches, P_3, P_3^*, H_2, and H_2^* bifurcating from $RS_{3:4}$. Close to $RS_{3:4}$ the solutions on these branches have eight switching points per period; examples are shown in fig. 9(b)–(d). Each of the branches then undergoes a saddle-node bifurcation; the branches remain unstable (i.e., some Floquet multipliers remain outside the unit disc). The branches that start at the saddle-node bifurcations SN_4 and SN_5, that is, P_4 and H_3, then end along with their asymmetric counterparts at the pitchfork bifurcations PF_3 and PF_4 on $\tilde{G}$, respectively.

The behaviour described above is seen at all resonance points on the branches of lens solutions with a resonance p:$q \geq 1$:2. That is, out of each resonance point four branches emerge (two branches of potato solutions and two branches of heart solutions), which then undergo a saddle-node bifurca-

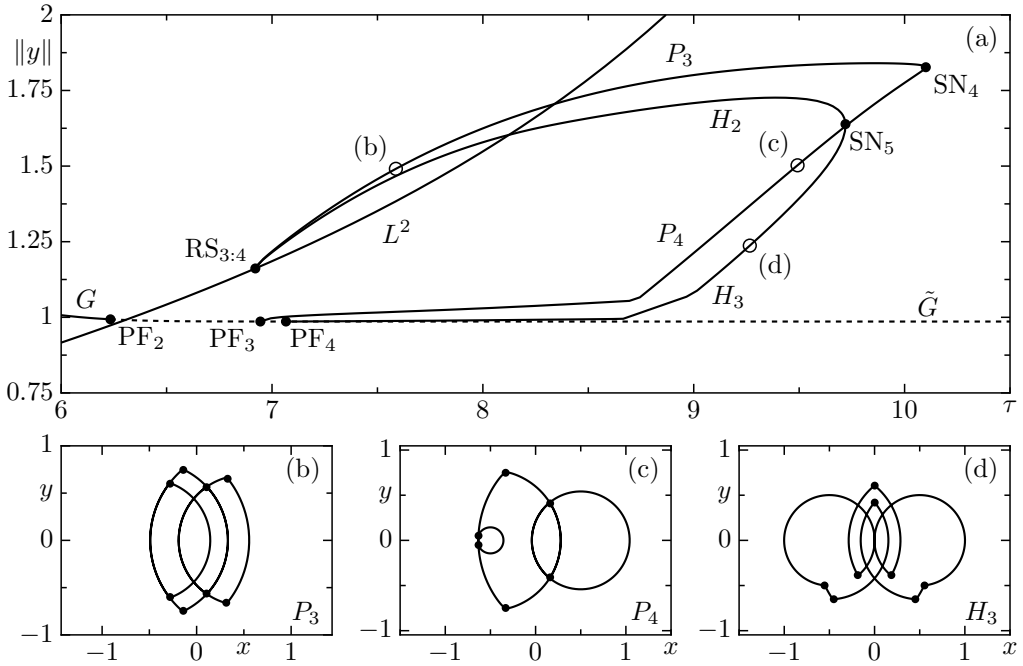

Figure 9. Panel (a) shows two branches of potato solutions P_3 and P_3^* along with two branches of heart solutions H_2 and H_2^*. These branches each undergo a saddle-node bifurcation before merging with the branch G of glasses solutions at a pitchfork bifurcation. Panels (b), (c) and (d) are examples of solutions at points along the branches.

tion and subsequently end at a pitchfork bifurcation on the branch $\tilde{G}$. Again the number of switching points per period of the solutions depends on the resonance point from which the branch bifurcates.

In the non-smooth limit $\varepsilon = 0$ of (2) the region of the branch of glasses solutions $\tilde{G}$ denoted by a dashed line in fig. 9(a) does not exist. It is from this branch that P_4 and H_3 bifurcate at pitchfork bifurcations. This leaves the question: what happens to P_4 and H_3 as $\varepsilon \to 0$?

Figure 10 shows an answer to this question with a series of one-parameter continuations for decreasing values of ε. The superscript of the branch and bifurcation labels denotes the value of ε used, which is halved each time. Figure 10 shows that, as the value of ε is decreased, the bifurcations PF_2 and PF_3 converge to the point $\tau = 2\pi$. In the non-smooth system (1) the branch G terminates at exactly $\tau = 2\pi$. This suggests that, as the smoothing of (2) is decreased, the bifurcations along $\tilde{G}$ accumulate at the point $\tau = 2\pi$.

Figure 11 shows the magnitude of the Floquet multipliers along the branches G and $\tilde{G}$. This further backs up our observations that the bifurcations accumulate to a point. Indeed as $\varepsilon \to 0$, on the range $6 < \tau < 7.2$, increasingly many Floquet multipliers cross the unit disc at $+1$. These crossings of the unit disc

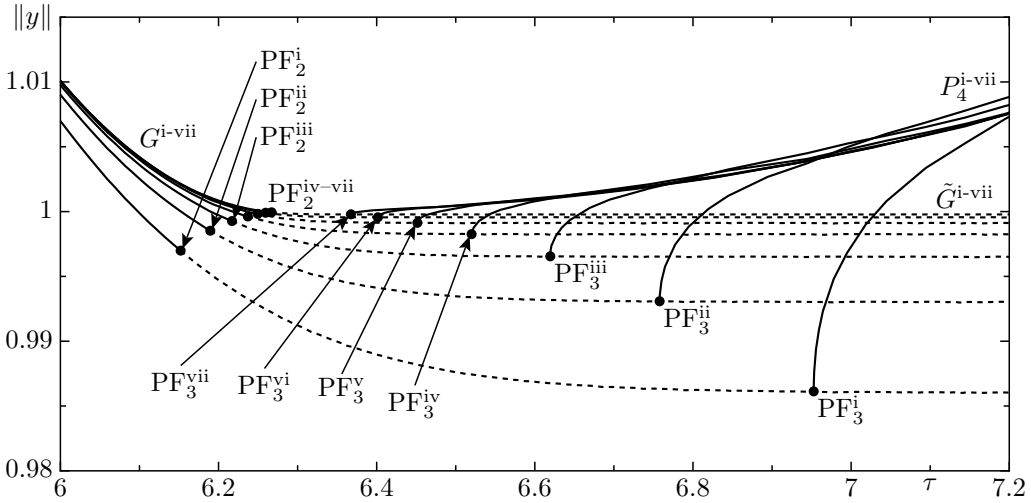

Figure 10. This figure shows a series of one-parameter continuations about the pitchfork bifurcation PF_3 for a range of ε values ($\varepsilon^{\mathrm{i}} = 0.01$, $\varepsilon^{\mathrm{ii}} = 0.005$, $\varepsilon^{\mathrm{iii}} = 0.0025$, etc.). As the value of ε decreases the parameter value that the pitchfork bifurcation PF_3 occurs at converges to $\tau = 2\pi$.

correspond to the pitchfork bifurcations that lie at the end of the branches bifurcating from resonance points on the branches of lens solutions (e.g., $\mathrm{RS}_{3:4}$ and $\mathrm{RS}_{5:6}$). There are infinitely many secondary branches of lens solutions and corresponding resonance points and, consequently, infinitely many bifurcations occur on $\tilde{G}$. Thus as $\varepsilon \to 0$ and all these bifurcations accumulate to a point, there are infinitely many branches bifurcating from a single point in the non-smooth system (1), the end point of G.

4.4 *Summary of connections between the branches*

Figure 12 combines the results of the previous two sections to show the combinations of the connections between the different resonance points. Each row shows the resonance points on a particular branch of lens solutions and the corresponding bifurcation on a branch of glasses solutions to which it connects. From fig. 12 we see that each of the resonance points on the branches of glasses solutions is connected to a resonance point on a branch of lens solutions. However the converse is not true; the resonance points on the branches of lens solutions with a resonance $p{:}q \geq 1{:}2$ are connected to a pitchfork bifurcation instead.

Figure 13(a) shows a single global picture of the branches and resonance points of (2). To prevent the figure from being unintelligible, some branches are omitted (each resonance point has two branches bifurcating from it). The regions marked (b)–(d) are shown in figs. 3, 7 and 9 respectively. The primary

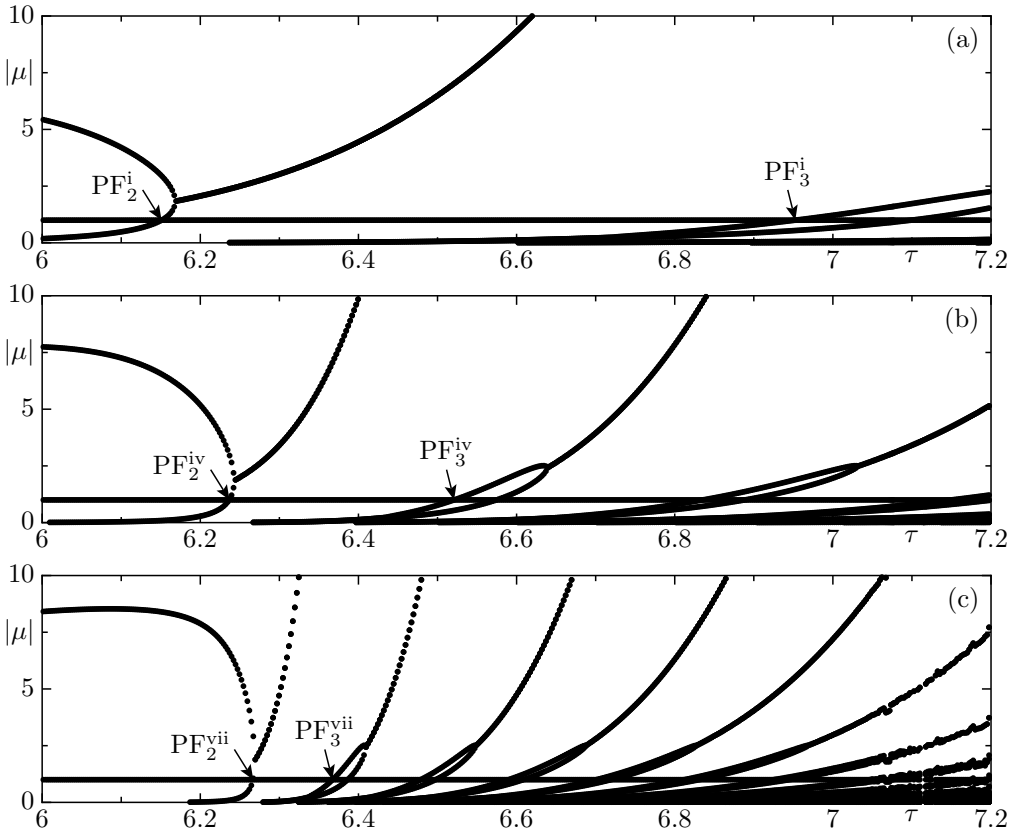

Figure 11. Panels (a), (b) and (c) show the Floquet multipliers along the branch G for decreasing values of ε. As the value of ε is decreased there is an accumulation of bifurcations close to $\tau = 2\pi$. The value of ε used in (c) is close to the computation limits of DDE-BIFTOOL as seen by the noise in the Floquet multipliers for $\tau > 7$

branches $P_{1,2}$ and H_1 can be seen in region (b) (cf., fig. 3(a)) where they bifurcate from G and L. Their secondary branches can also be seen bifurcating from G^3 and L^3, and G^5 and L^5. The secondary branches appear 'stretched' in τ.

All the smooth bifurcations, e.g., the resonance points, of the non-smooth system (1) are preserved by the smoothing of the system, whereas the dynamics in the vicinity of the non-smooth bifurcations of (1) changes significantly under smoothing. However, the manner in which the dynamics changes as (1) is smoothed is strictly controlled; the non-smooth bifurcation is 'stretched' to become the branch $\tilde{G}$ in the non-smooth system. As such, the smoothing still gives valuable information about the dynamics of the non-smooth system.

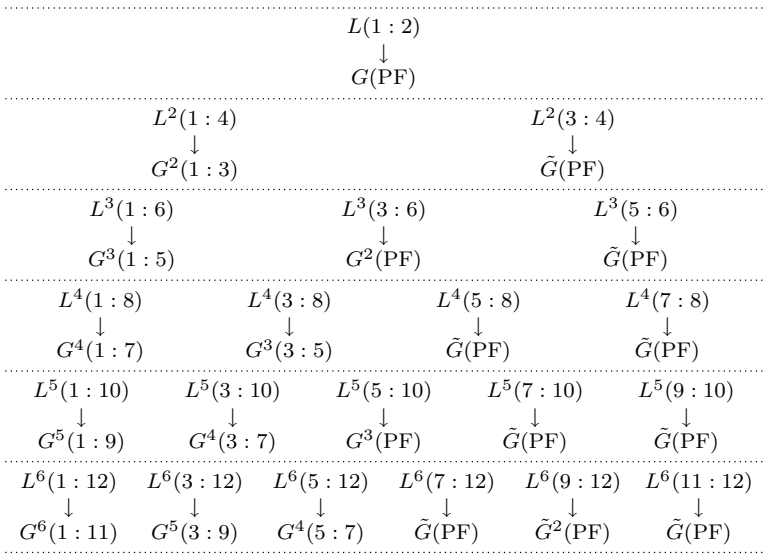

Figure 12. The connections between resonance points on the branches of lens and glasses solutions. Each row corresponds to all the resonance points along a particular branch of lens solutions, e.g., $L^2(1:4) \to G^2(1:3)$ is the connection between $\mathrm{RS}_{1:4}$ on L^2 to $\mathrm{RS}_{1:3}$ on G^2 (see fig. 9).

5 Conclusions

We presented a comprehensive picture of the dynamics of a non-smooth delay differential equation. This was achieved by using solution construction techniques for the non-smooth system hand-in-hand with a numerical bifurcation study of a related smoothed system. The dynamics of the non-smooth DDE under consideration are significantly more complex than previously thought. We found many new solution branches, stable and unstable, that bifurcate from previously unknown resonance points that are connected in an interesting combinatorial structure. In particular the extra branches give insight into how a non-smooth bifurcation in the non-smooth system is unfolded when the system is smoothed. This occurs in a controlled manner and, consequently, the smoothed system gives valuable knowledge on the original non-smooth system.

While we understand the overall combinatorics, as yet we are unable to show *why* particular resonance points are connected by solution branches. Since the periods of all the solutions are a multiple of the time delay (this multiple is dependent on the branch under consideration), it seems possible to make an argument based on the relationship between the periods of solutions at resonance points. However, rescaling (1) to give a unit time delay (and so introducing an extra parameter to the system) shows that it is not possible to make this argument work, because all the solutions on the connecting branches have the same period under this rescaling. Instead, to determine why

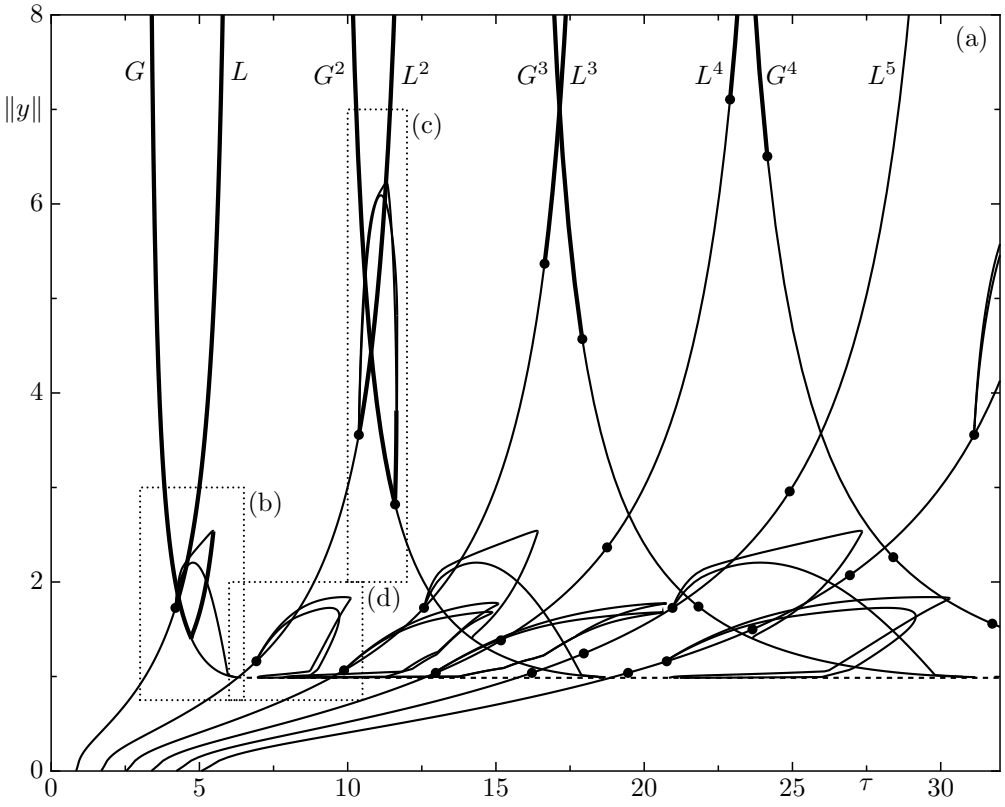

Figure 13. The branch structure of (2). Resonance points are marked with a dot and the branches of lens and glasses solutions are labelled (cf., fig. 6). All other branches are potato or heart solution branches. The marked regions (b)–(d) correspond to figs. 3, 7 and 9 respectively. Some branches are omitted for clarity (each resonance point has two branches bifurcation from it).

particular resonance points are connected, it appears that the actual solution construction, and how it changes as τ is varied, must be considered. This is a topic of ongoing research.

The approach taken in this paper can also be used in the setting of general piecewise-smooth DDEs. Models arising from relay control are one possible future application; a class of examples are piecewise-smooth DDEs [15] of the general form

$$\ddot{x}(t) + \alpha\dot{x}(t) + \beta x(t) = \begin{cases} a & \text{if } x(t-\tau) \leq 0, \\ b & \text{if } x(t-\tau) > 0. \end{cases}$$

Especially when explicit solutions cannot be constructed, the bifurcation analysis of a suitably smoothed DDE still promises valuable insight into the dynam-

ics of the equation. Smoothing has been considered in the literature primarily for non-smooth ODEs. Exploiting smoothing for general non-smooth DDEs remains an interesting direction for future research.

Finally, we mention that the study of non-smooth DDEs may help in the numerical bifurcation analysis of a given smooth DDE arising from a particular application. A significant problem in the smooth setting is the need for suitable starting solutions. If the smooth DDE can be reduced to an appropriate non-smooth limit then it may be possible to construct explicit solutions from which to start the analysis of the original DDE. The amount of smoothing would enter the problem as an additional continuation parameter.

References

[1] U. an der Heiden, A. Longtin, M.C. Mackey, and J.G. Milton, *Oscillatory modes in a nonlinear second-order differential equation with delay*, Journal of Dynamics and Differential Equations **2** (1990), no. 4, 423–449.

[2] U. an der Heiden and K. Reichard, *Multitude of oscillatory behaviour in a nonlinear second order differential-difference equation*, Z. angew. Math. Mech **70** (1990), no. 6, T621–T624.

[3] S. Bannerjee and G. Verghese, *Nonlinear phenomena in power electronics*, IEEE press, 2001.

[4] D.A.W. Barton, B. Krauskopf, and R.E. Wilson, *Explicit periodic solutions in a model of a relay controller with delay and forcing*, BCANM Preprint 2004.25, 2004.

[5] W. Bayer and U. an der Heiden, *Oscillation types and bifurcations of a nonlinear second-order differential-difference equation*, Journal of Dynamics and Differential Equations **10** (1998), no. 2, 303–326.

[6] B. Brogliato, *Impacts in mechanical systems — analysis and modelling*, Lecture notes in physics, vol. 551, Springer-Verlag, 2000.

[7] L.C. Davis, *Modification of the optimal velocity traffic model to include delay due to driver reaction time*, Physica A **319** (2002), 557–567.

[8] M. di Bernardo, C. Budd, A.R. Champneys, P. Kowalczyk, A.B. Nordmark, G. Olivar, and P.T. Piiroinen, *Bifurcations in nonsmooth dynamical systems*, BCANM Preprint 2005.04.

[9] O. Diekmann, S. van Gils, S.M.V. Lunel, and H.-O. Walther, *Delay equations: functional-, complex-, and nonlinear analysis*, Applied Mathematical Sciences, vol. 110, Springer, 1995.

[10] K. Engelborghs, T. Luzyanina, and G. Samaey, *DDE-BIFTOOL v. 2.00: a Matlab package for bifurcation analysis of delay differential equations*, Tech. Report TW-330, Department of Computer Science, K.U.Leuven, Leuven, Belgium, 2001.

[11] E. Fridman, L. Fridman, and E. Shustin, *Steady modes in relay control systems with time delay and periodic disturbances*, Journal of Dynamic Systems, Measurement, and Control **122** (2000), 732–737.

[12] L. Fridman, E. Fridman, and E. Shustin, *Steady modes and sliding modes in relay control systems with delay*, Sliding mode control in engineering (J.P. Barbot and W. Perruguetti, eds.), Marcel Dekker, New York, 2002, pp. 263–293.

[13] J.-L. Gouzé and T Sari, *A class of piecewise linear differential equations arising in biological models*, Dynamical systems **17** (2003), 299–316.

[14] J.K. Hale and S.M.V. Lunel, *Introduction to functional differential equations*, Applied Mathematical Sciences, no. 99, Springer-Verlag, 1993.

[15] U. Holmberg, *Relay feedback of simple systems*, Ph.D. thesis, Lund Institute of Technology, 1991.

[16] V. Kapila, W.M. Haddad, and A. Grivas, *Stabilization of linear systems with simultaneous state, actuation, and measurement delays*, International Journal of Control **72** (1999), no. 18, 1619–1629.

[17] L.E. Kollár, G. Stépán, and J. Turi, *Dynamics of delayed piecewise linear systems*, Proceedings of the fifth Mississippi state conference on differential equations and computational simulations, 2001.

[18] R.I. Leine and H. Nijmeijer, *Dynamics and bifurcations of non-smooth mechanical systems*, Lecture notes in applied and computational mechanics, vol. 18, Springer, 2004.

[19] J.G. Milton and A. Longtin, *Evaluation of pupil constriction and dilation from cycling measurements*, Vision Research **30** (1990), no. 4, 515–525.
[20] J. Nilsson, B. Bernhardsson, and B. Wittenmark, *Stochastic analysis and control of real-time systems with random time delays*, Automatica **34** (1998), no. 1, 57–64.
[21] J. Norbury and R.E. Wilson, *Dynamics of constrained differential delay equations*, Journal of Computational and Applied Mathematics **125** (2000), 201–215.
[22] K. Popp and P Stelter, *Stick-slip vibrations and chaos*, Philosophical Transactions: Physical Sciences and Engineering **332** (1990), no. 1624, 89–105.
[23] E. Shustin, E. Fridman, and L. Fridman, *Oscillations in a second-order discontinuous system with delay*, Discrete and continuous dynamical systems **9** (2003), no. 2, 339–358.
[24] J. Sieber, *Dynamics of delayed relay control systems with large delays*, Proceedings of 5th IFAC workshop on time-delay systems, 2004.
[25] G. Stépán, *Retarded dynamical systems*, Longman, 1989.
[26] M. Wiercigroch and B. de Kraker (eds.), *Applied nonlinear dynamics and chaos of mechanical systems with discontinuities*, World scientific series on nonlinear science: series A, vol. 28, World Scientific, 2000.
[27] Z.T. Zhubsubaliyev and E. Mosekilde, *Bifurcations and chaos in piecewise-smooth dynamical systems*, World scientific series on nonlinear science: series A, vol. 44, World Scientific, 2003.